

This is a repository copy of *Interlayer transmission of magnons in dynamic spin valve structures*.

White Rose Research Online URL for this paper:
<https://eprints.whiterose.ac.uk/161844/>

Version: Published Version

Article:

Chen, Qian, Ruan, Xuezhong, Yuan, Honglei et al. (5 more authors) (2020) Interlayer transmission of magnons in dynamic spin valve structures. *Applied Physics Letters*. 132403. ISSN 0003-6951

<https://doi.org/10.1063/1.5145182>

Reuse

Items deposited in White Rose Research Online are protected by copyright, with all rights reserved unless indicated otherwise. They may be downloaded and/or printed for private study, or other acts as permitted by national copyright laws. The publisher or other rights holders may allow further reproduction and re-use of the full text version. This is indicated by the licence information on the White Rose Research Online record for the item.

Takedown

If you consider content in White Rose Research Online to be in breach of UK law, please notify us by emailing eprints@whiterose.ac.uk including the URL of the record and the reason for the withdrawal request.

Interlayer transmission of magnons in dynamic spin valve structures

Cite as: Appl. Phys. Lett. **116**, 132403 (2020); <https://doi.org/10.1063/1.5145182>

Submitted: 15 January 2020 . Accepted: 14 March 2020 . Published Online: 30 March 2020

Qian Chen, Xuezhong Ruan, Honglei Yuan, Xiaochao Zhou , Zhaoxia Kou, Zhaocong Huang, Yongbing Xu, and Ya Zhai 



View Online



Export Citation



CrossMark

ARTICLES YOU MAY BE INTERESTED IN

[Spintronics with compensated ferrimagnets](#)

Applied Physics Letters **116**, 110501 (2020); <https://doi.org/10.1063/1.5144076>

[Spintronics on chiral objects](#)

Applied Physics Letters **116**, 120502 (2020); <https://doi.org/10.1063/1.5144921>

[Large spin Hall effect and increase in perpendicular magnetic anisotropy in artificially synthesized amorphous W/Hf multilayer/CoFeB system](#)

Applied Physics Letters **116**, 132401 (2020); <https://doi.org/10.1063/5.0002642>

Lock-in Amplifiers
up to 600 MHz



Watch



Interlayer transmission of magnons in dynamic spin valve structures

Cite as: Appl. Phys. Lett. **116**, 132403 (2020); doi: [10.1063/1.5145182](https://doi.org/10.1063/1.5145182)

Submitted: 15 January 2020 · Accepted: 14 March 2020 ·

Published Online: 30 March 2020





View Online



Export Citation



CrossMark

Qian Chen,¹ Xuezhong Ruan,² Honglei Yuan,^{1,3} Xiaochao Zhou,¹  Zhaoxia Kou,¹ Zhaocong Huang,¹ Yongbing Xu,^{2,4} and Ya Zhai^{1,a)} 

AFFILIATIONS

¹School of Physics, Southeast University, Nanjing 211189, People's Republic of China

²Jiangsu Provincial Key Laboratory of Advanced Photonic and Electronic Materials, School of Electronic Science and Engineering, Nanjing University, Nanjing 210093, People's Republic of China

³School of Physics and Telecommunication Engineering, Zhoukou Normal University, Zhoukou 466001, China

⁴York-Nanjing International Joint Center in Spintronics, Department of Electronics, The University of York, York YO10 5DD, United Kingdom

^{a)} Author to whom correspondence should be addressed: yazhai@seu.edu.cn

ABSTRACT

Magnonic devices are promising alternatives to conventional charge-current-driven spintronic devices. As the basic unit of spintronic devices, the spin valve is of limited use in magnonics because its dynamics is rarely studied. Here, we investigate the interlayer transmission of magnons in dynamic spin valve structures using the time-resolved magneto-optical Kerr effect. Interaction between magnons and the interfacial dissipation are studied by comparing three samples with different spin valve structures. Magnons with different intrinsic frequencies have strong interactions. In contrast, magnons with similar intrinsic frequencies have relatively weak interactions. Interfacial dissipations of magnons are increased by rare earth insertion, which can reduce the interactions between magnons indirectly. This work extends the application of spin valve structures to magnonic devices beyond their conventional use.

Published under license by AIP Publishing. <https://doi.org/10.1063/1.5145182>

The spin valve (SV) structure, consisting of one layer of a non-magnetic material sandwiched between two magnetic layers, has been widely used in spintronic devices because of its giant magnetoresistance (GMR).^{1–4} The parallel magnetization orientation of the two magnetic layers corresponds to the low-resistance state, while the anti-parallel orientation represents the high-resistance state. However, dynamic properties of such a structure are rarely studied.^{5,6} When one of the magnetic layers in the SV structure is in a dynamic state, spin current is pumped into the nonmagnetic material, and consequently, it interacts with the other magnetic layer.^{7–9} During this process, magnons, the quanta of spin waves, will be excited, spread, and dissipated between layers. Recently, a new concept, magnon valve, was initially put forward by Wu *et al.*,¹⁰ in which the magnon current transmission coefficient could be controlled by the relative orientation of two ferromagnetic layers. In their study, magnon-spin interconversion is used to control angular momentum transport in yttrium iron garnet (YIG)/Au/YIG magnon valves. Later, Guo *et al.*¹¹ achieved the pure magnon valve with YIG/NiO/YIG sandwiches, in which pure magnon current can be controlled by magnetic states of the two magnetic insulating

layers. A similar phenomenon was also reported by Cramer *et al.*¹² in YIG/CoO/Co structures, which was regarded as the magnon spin valve effect determined by the different effective spin Hall angles of Co when the magnetization direction of Co changes. These findings are considered as the focus in spintronics, which may lead to a new type of circuitry that is faster and more efficient than traditional electronics. Very recently, magnon-torque-induced magnetization switching through an antiferromagnetic insulator was archived by Wang *et al.*¹³ and Wang *et al.*¹⁴ They demonstrated that the magnon torque is sufficient to control the magnetization, which is comparable with traditional electrical spin torque ratios. Also, pioneering works on spin orbit torque (SOT) switching for TmIG/Pt¹⁵ and YIG/Pt¹⁶ indicated that spin torque inside the magnetic insulator can only be magnon-mediate. These studies inspire us to explore the interlayer transmission of magnons in dynamic SV structures.

In this manuscript, we study the transmission of magnons between layers in SV structures. Magnons with different intrinsic frequencies are excited in different magnetic layers by the time-resolved magneto-optical Kerr effect (TR-MOKE).^{17–19} It is found that the

interactions between magnons and interfacial dissipation should be taken into account in this type of structure. Interactions between magnons are strong when intrinsic frequencies of magnons show a large difference. For magnons with similar intrinsic frequencies, their interactions are relatively weak. In addition, the effect of interfacial dissipation can be increased by rare earth (RE) insertion, and the increased interfacial dissipation will consequently result in the decrease of magnon interactions.

Three stacks of spin-valve multilayers are deposited on silicon dioxide substrates at room temperature by magnetron sputtering under a base pressure of 1.5×10^{-5} Pa. The structures are schematically displayed in Figs. 1(a), 3(a), and 4(a), where sample A is composed of Ta(3)/Py(4)/Cu(2)/Fe₅₀Co₅₀(4)/Ta(1), sample B is Ta(3)/Py(4)/Cu(2)/Py(4)/Ta(1), and sample C is Ta(3)/Py(4)/Tb(1)/Cu(2)/Fe₅₀Co₅₀(4)/Gd(1)/Ta(1) (all thicknesses in nm). Two ferromagnetic materials Py and FeCo are selected here because the saturation magnetization of FeCo is nearly double that of Py, leading to a visible difference in their intrinsic frequencies. Cu is the most commonly used nonmagnetic layer for spin-valve structures, and Ta is used as a buffer and capping layer. Such a structural design enables TR-MOKE studies on the effects of each of the magnetic layers. Magnetic hysteresis loops of sample A and sample C are measured using a vibrating sample magnetometer. Both hysteresis loops display a two-step-switching behavior, suggesting a magnetic decoupling of the two TM layers by the Cu spacer, which is consistent with previous studies.²⁰ Two coercivity values $H_{C,Py}$ and $H_{C,FeCo}$ of the loops are obtained, corresponding to the Py and FeCo layers. Comparing the loops of samples A and C, we find that upon insertion of the Tb and Gd layers, the magnitudes of both $H_{C,Py}$ and $H_{C,FeCo}$ increase, from 5 Oe to 10 Oe for the Py layer and from 9 to 48 for FeCo layers, indicating the effect of RE insertions. During the TR-MOKE detection, laser pulses of ~ 50 fs from a Ti:sapphire regenerative amplifier with a repetition rate of 1 kHz at a central wavelength of 800 nm are split into a stronger pump and weaker probe. The pump pulse is focused on a spot of $\sim 500 \mu\text{m}$ in diameter on the sample surface, while the focused spot of the probe is $\sim 200 \mu\text{m}$ in diameter and is located at the center of the pump spot. The polar Kerr rotation of the probe reflected from the sample surface is detected by a balanced optical bridge and measured using a lock-in amplifier, which is synchronized to an optical chopper that modulates the pump beam. The external magnetic field H generated by an

electromagnet is applied at $\varphi = 50^\circ$ with respect to the surface normal. The strength of H is controlled by electrical current and calibrated by a Gauss meter. All the measurements are performed at room temperature.

In response to the laser pulses, the magnetization is triggered to a state of free precession. Due to the combination of the exchange interaction and the spin-orbit interaction in ferromagnetic materials, the laser-induced magnetization dynamics results in an oscillatory TR-MOKE signal. Kerr signals of Sample A under different values of external magnetic fields are shown in Fig. 1(b), where we can see that the damped oscillations last for about hundreds of picoseconds. Obvious oscillations occur in all transient traces, indicating the efficient excitation of magnons. At each field, the time-dependent Kerr signal is converted into the frequency domain using a fast Fourier transformation (FFT) algorithm, as shown in Fig. 1(c). In each spectrum, two modes occur, and both shift to higher frequency with increasing external field. The mode in the lower frequency domain with weaker intensity represents magnons excited in Py layer underneath, while the mode in the higher frequency domain with stronger intensity represents magnons excited in FeCo. To analyze the data quantitatively, the oscillatory components in the magnetization dynamics are fitted by using the following damped harmonic sum function:²¹

$$\theta_{Kerr} = A_{Py} \exp(-t/\tau_{Py}) \sin(2\pi f_{Py} t + \varphi_{Py}) + A_{FeCo} \exp(-t/\tau_{FeCo}) \sin(2\pi f_{FeCo} t + \varphi_{FeCo}) + B(t), \quad (1)$$

where A_{Py} , τ_{Py} , f_{Py} , and φ_{Py} (A_{FeCo} , τ_{FeCo} , f_{FeCo} , and φ_{FeCo}) are the amplitude, lifetime, frequency, and initial phase of magnons in Py (FeCo), respectively. The background term $B(t)$ accounting for the slower demagnetization recovery is generally a summation of one or two exponential functions.

The field dependence of frequencies $f_{Py}(H)$ and $f_{FeCo}(H)$ given by the best fitting of sample A is shown in Fig. 2. The extracted results are almost identical to that obtained by FFT spectrum. Dashed lines in

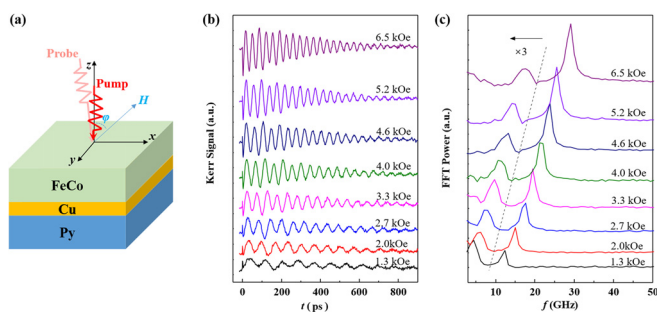


FIG. 1. (a) Schematic structure of sample A and the TR-MOKE measurement geometry. (b) Laser-induced magnetization dynamics of sample A under different values of external magnetic fields. (c) FFT spectrum for the oscillatory components in (b). The portion of the spectrum to the left of the dashed line is amplified by three times.

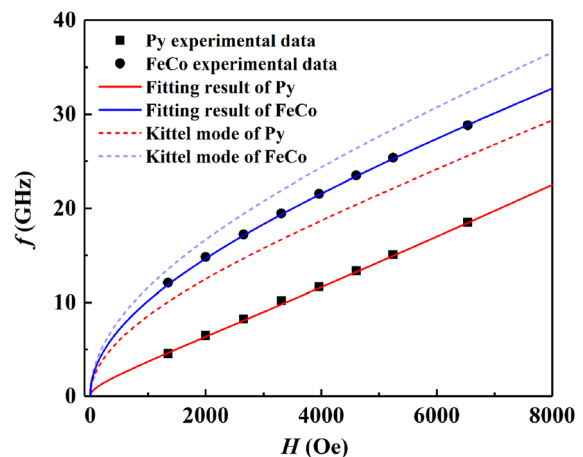


FIG. 2. Field dependence of frequencies f_{Py} (filled squares) and f_{FeCo} (filled circles) of sample A. Dashed lines denote the calculated values of the Kittel mode with Eq. (2). Red and blue solid lines are best dispersion fittings of Py and FeCo magnet with Eq. (4).

Fig. 2 denote the calculated values of the Kittel mode derived from the Landau-Lifshitz-Gilbert (LLG) equation, and the formula is expressed as^{21–24}

$$\omega_{\text{Kittel}}^2 = \omega_H(\omega_H + \omega_{FM}\sin^2(\theta)), \quad (2)$$

where $\omega_H = \gamma H \sin\phi / \sin\theta$ and $\omega_{FM} = 4\pi\gamma M_{\text{eff}}$. γ and M_{eff} are the gyromagnetic ratio and the effective magnetization of corresponding ferromagnetic layer. θ is the angle of the equilibrium magnetization with respect to the normal of film plane, which meets the following equation of minimum free energy:

$$2H\sin(\theta - \phi) - 4\pi M_{\text{eff}}\sin 2\theta = 0. \quad (3)$$

From Fig. 2, we can see that the detected frequencies of Py and FeCo are much smaller than the calculated results of Kittel modes. We hypothesize that such a decay of frequency may come from two factors: the dissipation of interfaces and the interactions between magnons. Here, the interfacial dissipation factors of the two ferromagnetic layers FM1 and FM2 in SV structure are introduced as δ_{FM1} and δ_{FM2} ($0 < \delta < 1$), and the interaction between magnons from FM1 and FM2 can be equivalent to $\omega_I = 4\pi\gamma(1 - \delta_{FM1})M_{FM1} \times (1 - \delta_{FM2})M_{FM2} / [(1 - \delta_{FM1})M_{FM1} + (1 - \delta_{FM2})M_{FM2}]$, where M_{FM1} and M_{FM2} are the effective magnetization of FM1 and FM2, respectively. Considering these effects, Eq. (2) can be revised as

$$\begin{aligned} \omega_{FM1}^2 &= \omega_H[\omega_H + (1 - \delta_{FM1})\omega_{FM1}\sin^2(\theta) + \omega_I\sin^2(\theta)], \\ \omega_{FM2}^2 &= \omega_H[\omega_H + (1 - \delta_{FM2})\omega_{FM2}\sin^2(\theta) + \omega_I\sin^2(\theta)]. \end{aligned} \quad (4)$$

Best fittings are plotted in Fig. 2 by solid lines which agree very well with the experimental results. It gives $\delta_{Py} = 0.575$ and $\delta_{FeCo} = 0.002$, denoting that the interfacial dissipation effect for magnons excited from the underneath Py layer is relatively strong, while that for magnons excited from the upper FeCo layer is almost negligible. This is reasonable because during the interlayer transmission of Py magnon, three interfaces Py/Cu, Cu/FeCo, and FeCo/Ta take effect; nevertheless for FeCo magnon, the main effect is the FeCo/Ta interface. The equivalent interactions between magnons can be calculated as 78.8 GHz for Py magnon and 65.9 GHz for FeCo magnon. According to the above formulas, interactions between magnons are related to their intrinsic frequencies, which are mainly determined by the effective magnetization of FM layers, and will also be affected by interfacial dissipations. When there is a large difference between intrinsic frequencies of magnons, the interaction is large. When the intrinsic frequencies of magnons are close (or the same), their interactions become weak. To further demonstrate this theory, we design sample B (Ta/Py/Cu/Py/Ta) and sample C (Ta/Py/Tb/Cu/FeCo/Gd/Ta) for comparison.

The schematic structure of sample B and typical TR-MOKE spectra are illustrated in Figs. 3(a) and 3(b). The Kerr signal of sample B is weaker than sample A because the satisfied magnetization of Py is much smaller than FeCo. Although two Py layers in sample B at different locations experience different interfacial dissipations, their intrinsic frequencies are similar. Therefore, it is difficult to separate them from each other by neither nonlinear fitting nor FFT. Here, we fit the Kerr signal of sample B by one branch of the damped harmonic function as shown in Eq. (1). As plotted by solid lines in Fig. 3(b), the fitted curves agree well with experiments, and the extracted frequencies and lifetime of Py magnons at various external fields are shown in Figs. 3(c) and 3(d). Frequencies extracted from sample B are larger than those

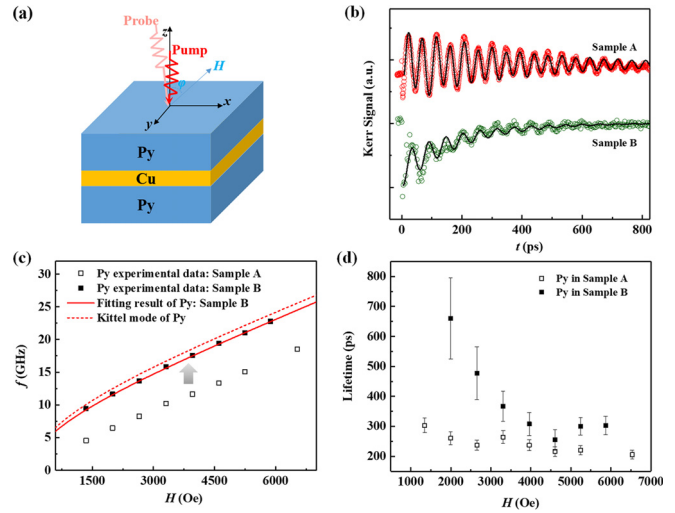


FIG. 3. (a) Schematic structure of sample B. (b) TR-MOKE spectra of sample A and sample B measured at 3961 Oe. Solid lines are best fittings. (c) Frequencies of Py in sample B (filled squares) compared with sample A (hollow squares). The dashed line denotes the calculated values of the Kittel mode of Py. The red solid line is the best dispersion fitting of Py in sample B. (d) Lifetime of Py magnon in sample B (filled squares) and sample A (hollow squares).

extracted from sample A and close to the Kittel mode of Py. The lifetime of Py magnon in sample A at each field is always smaller than that in sample B and close to the values obtained in Pt/Py (2 nm)/Pt by Mizukami *et al.*,²⁵ where spin current is damped in Pt because of spin pumping. It suggests that dissipation of spin current also occurs in our structures and is more serious in sample A than sample B. By fitting the field dependence of the extracted frequencies with Eqs. (3) and (4), we obtain the interfacial dissipation factors of the upper and lower Py layers, which are 0.001 and 0.640, respectively. The equivalent interaction between magnons is about 54.9 GHz, which is much smaller than that obtained in sample A and consists with our speculation.

Figure 4(a) shows the schematic structure of sample C. In this structure, we try to change the interfacial dissipation by capping RE layers on ferromagnetic layers. Here, we choose RE elements, Tb and Gd as insert layers because a similar structure has been studied in our previous study,²⁰ in which an antiferromagnetic coupling between the ferromagnetic and RE nanolayers was found and an antiferromagnetic interface can be induced. We speculate that such an antiferromagnetic interface may lead to an increasing of the interfacial dissipation. Typical TR-MOKE spectra are shown in Fig. 4(b). The Kerr signal of sample C is weaker than that of sample A, suggesting a stronger dissipation of magnons in sample C. Figure 4(c) shows the field dependence of extracted frequencies of Py and FeCo in sample C. It is interesting that the frequency of Py magnon decreases a lot compared with sample A, while the frequency of FeCo is increased and almost overlaps with its Kittel mode. The reason probably is that as the interfacial dissipation increases, the interactions between Py and FeCo magnons are suppressed. For Py magnons, the dominant effect is the increased interfacial dissipation. In order to verify this, we fit the experimental results by Eq. (4) as illustrated by solid lines in Fig. 4(c).

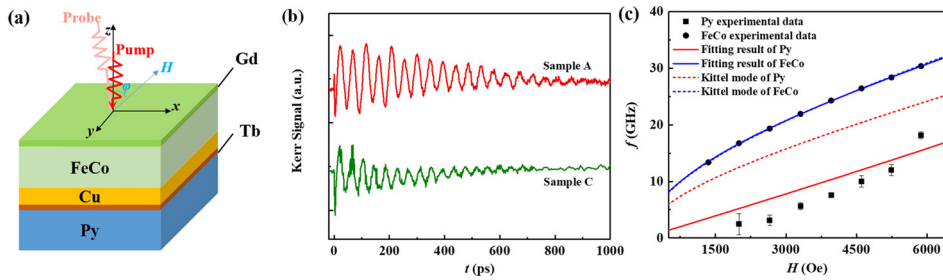


FIG. 4. (a) Schematic structure of sample C and the TR-MOKE measurement geometry. (b) Typical TR-MOKE spectra of sample A and sample C measured at 3961 Oe. (c) Frequencies of Py (filled squares) and FeCo (filled circles) in sample C. Dashed lines denote the calculated values of the Kittel mode. Red and blue solid lines are the best dispersion fitting of Py and FeCo, respectively.

TABLE I. The interfacial dissipation factors δ and the equivalent interactions between magnons ω_1 for the three types of spin valve structures. Py here in sample B refers to the lower layer.

Sample		ω_1 (GHz)	δ
FeCo	Sample A	65.9	0.002
	Sample C	20.0	0.110
Py	Sample A	78.7	0.575
	Sample B	54.9	0.640
	Sample C	21.5	0.900

We obtain $\delta_{Py} = 0.900$ and $\delta_{FeCo} = 0.110$, which are both larger than that in sample A. The equivalent interactions between magnons are 21.5 GHz for Py and 20.0 GHz for FeCo; both are much smaller than sample A as shown in Table I. These results demonstrate an increased interfacial dissipation caused by RE insertion and a consequent reduction of interactions between magnons.

To summarize, we have studied the effects of the magnon interactions and the interfacial dissipation in dynamic SV structures. The interfacial dissipation factors δ and the equivalent interactions between magnons ω_1 are obtained in three types of SV structures, and the results are summarized in Table I. Comparing sample B with sample A, we demonstrate that the interactions between magnons are related to their intrinsic frequencies. When intrinsic frequencies of magnons show a large difference, interactions between magnons are strong. When the intrinsic frequencies of magnons are similar, their interactions are relatively weak. Comparing sample C with sample A, we find that interfacial dissipation of magnons can be increased by RE insertion; as a result, interactions between Py and FeCo magnons are reduced. Our research extends the application of SV structures in magnonics.

AUTHORS' CONTRIBUTIONS

Q.C. and X.R. contributed equally to this work.

This work was supported by the National Key Research and Development Program of China (Grant Nos. 2017YFA0204800 and 2016YFA0300803), the National Natural Science Foundation of China (Grant Nos. 51571062, 61427812, 11504047, 11774160, and 51702380), the Natural Science Foundation of Jiangsu Province of China (Grant No. BK20192006), and the Fundamental Research Funds for the Central Universities (Grant No. 021014380113).

REFERENCES

- B. Dieny, V. S. Speriosu, S. S. P. Parkin, B. A. Gurney, D. R. Wilhoit, and D. Mauri, *Phys. Rev. B* **43**, 1297 (1991).
- D. J. Monsma, J. C. Lodder, T. J. A. Popma, and B. Dieny, *Phys. Rev. Lett.* **74**, 5260 (1995).
- R. W. Cross, Y. K. Kim, J. O. Oti, and S. E. Russek, *Appl. Phys. Lett.* **69**, 3935 (1996).
- F. J. Jedema, A. T. Filip, and B. J. van Wees, *Nature* **410**, 345 (2001).
- R. Urban, G. Woltersdorf, and B. Heinrich, *Phys. Rev. Lett.* **87**, 217204 (2001).
- B. Heinrich, Y. Tserkovnyak, G. Woltersdorf, A. Brataas, R. Urban, and G. E. W. Bauer, *Phys. Rev. Lett.* **90**, 187601 (2003).
- F. D. Czeschka, L. Dreher, M. S. Brandt, M. Weiler, M. Althammer, I.-M. Imort, G. Reiss, A. Thomas, W. Schoch, W. Limmer *et al.*, *Phys. Rev. Lett.* **107**, 046601 (2011).
- Y. Tserkovnyak, A. Brataas, and G. E. W. Bauer, *Phys. Rev. B* **66**, 224403 (2002).
- H. J. Jiao and G. E. W. Bauer, *Phys. Rev. Lett.* **110**, 217602 (2013).
- H. Wu, L. Huang, C. Fang, B. S. Yang, C. H. Wan, G. Q. Yu, J. F. Feng, H. X. Wei, and X. F. Han, *Phys. Rev. Lett.* **120**, 097205 (2018).
- C. Y. Guo, C. H. Wan, X. Wang, C. Fang, P. Tang, W. J. Kong, M. K. Zhao, L. N. Jiang, B. S. Tao, G. Q. Yu, and X. F. Han, *Phys. Rev. B* **98**, 134426 (2018).
- J. Cramer, F. Fuhrmann, U. Ritzmann, V. Gall, T. Niizeki, R. Ramos, Z. Qiu, D. Hou, T. Kikkawa, J. Sinova *et al.*, *Nat. Commun.* **9**, 1089 (2018).
- H. Wang, J. Finley, P. Zhang, J. Han, J. T. Hou, and L. Liu, *Phys. Rev. Appl.* **11**, 044070 (2019).
- Y. Wang, D. Zhu, Y. Yang, K. Lee, R. Mishra, G. Go, S. Oh, D. Kim, K. Cai, E. Liu *et al.*, *Science* **366**, 1125 (2019).
- C. O. Avci, A. Quindeau, C. F. Pai, M. Mann, L. Caretta, A. S. Tang, M. C. Onbasli, C. A. Ross, and G. S. D. Beach, *Nat. Mater.* **16**, 309 (2017).
- C. Y. Guo, C. H. Wan, M. K. Zhao, H. Wu, C. Fang, Z. R. Yan, J. F. Feng, H. F. Liu, and X. F. Han, *Appl. Phys. Lett.* **114**, 192409 (2019).
- B. Koopmans, M. van Kampen, J. T. Kohlhepp, and W. J. M. de Jonge, *Phys. Rev. Lett.* **85**, 844 (2000).
- G. P. Zhang, W. Hubner, G. Lefkidis, Y. H. Bai, and T. F. George, *Nat. Phys.* **5**, 499 (2009).
- G. Woltersdorf, M. Buess, B. Heinrich, and C. H. Back, *Phys. Rev. Lett.* **95**, 037401 (2005).
- W. Zhang, D. Zhang, P. K. J. Wong, H. L. Yuan, S. Jiang, G. van der Laan, Y. Zhai, and Z. H. Lu, *ACS Appl. Mater. Interfaces* **7**, 17070 (2015).
- Z. F. Chen, Y. Yan, S. F. Li, X. G. Xu, Y. Jiang, and T. S. Lai, *Sci. Rep.* **7**, 42513 (2017).
- S. Mizukami, F. Wu, A. Sakuma, J. Walowski, D. Watanabe, T. Kubota, X. Zhang, H. Naganuma, M. Oogane, Y. Ando *et al.*, *Phys. Rev. Lett.* **106**, 117201 (2011).
- S. Iihama, S. Mizukami, H. Naganuma, M. Oogane, Y. Ando, and T. Miyazaki, *Phys. Rev. B* **89**, 174416 (2014).
- B. Liu, X. Ruan, Z. Wu, H. Tu, J. Du, J. Wu, X. Lu, L. He, R. Zhang, and Y. Xu, *Appl. Phys. Lett.* **109**, 042401 (2016).
- S. Mizukami, H. Abe, D. Watanabe, M. Oogane, Y. Ando, and T. Miyazaki, *Appl. Phys. Express* **1**, 121301 (2008).